Optical remote sensing of coastal waters from geostationary platforms: a feasibility study - Mapping Total Suspended Matter with SEVIRI

Griet Neukermans, Bouchra Nechad and Kevin Ruddick
Management Unit of the North Sea Mathematical Models (MUMM)
Royal Belgian Institute for Natural Sciences (RBINS)
Gulledelle 100
1200 Brussels
Belgium
(g.neukermans, b.nechad, k.ruddick + @mumm.ac.be)

ABSTRACT

Geostationary ocean colour sensors do not yet exist, but are under consideration by a number of space agencies. This study tests the feasibility and assesses the potential for optical remote sensing of coastal waters from geostationary platforms, with the existing SEVIRI (Spinning Enhanced Visible and InfraRed Imager) meteorological sensor on the METOSAT Second Generation platform. Data are available in near real time every 15 minutes. SEVIRI lacks sufficient bands for chlorophyll remote sensing but its spectral resolution is sufficient for quantification of Total Suspended Matter (TSM) in turbid waters, using a single broad red band, combined with a suitable near infrared band. A test data set for mapping of TSM was obtained from the SEVIRI Archive of the Royal Meteorological Institute of Belgium (RMIB), covering 15 consecutive days in September 2006 for the Southern North Sea. Atmospheric correction of SEVIRI images included corrections for Rayleigh and aerosol scattering, ozone absorption and atmospheric transmittances. A one-band TSM retrieval algorithm, calibrated by non-linear regression of seaborne measurements of TSM and water-leaving reflectance was applied. Results show that (1) mapping of TSM in the Southern North Sea is feasible with SEVIRI and that TSM maps are well correlated with TSM maps obtained from MODIS (2) during cloud-free days, high frequency dynamics of TSM are detected and (3) daily composites of TSM could be generated in partially cloudy weather.

INTRODUCTION

The general objective of this study is to test the feasibility and assess the potential for optical remote sensing of coastal waters from geostationary platforms. Since the launch of SeaWiFS in 1997 and MODIS-AQUA and ENVISAT-MERIS in 2002, ocean colour data from sensors on polar-orbiting platforms have become an established source of information for monitoring of chlorophyll *a* and total suspended matter (TSM) in coastal waters (International Ocean Colour Coordinating Group (IOCCG), 2000; Stumpf, 2001; Ruddick *et al.,* 2008*).* These sensors provide data in mid-latitudes with typical space and time resolution of about 1km and 1 day in cloud-free periods. While these sensors give an enormous advantage in terms of spatial coverage when compared to *in situ* measurement techniques, cloudiness is a severe restriction in many regions. The daily revisit may also be a limitation in coastal waters with high frequency dynamics related to tide- or wind-driven advection, resuspension or mixing/settling. For these two reasons the much higher temporal resolution that can be achieved from a geostationary platform is very attractive: if dynamics of the observed parameters are fast, a fast sampling frequency is necessary to resolve variability; if parameters vary little over the day then many

samples made at different times of the day will enable a more complete daily composite to be built up in the case where scattered clouds move through a region.

The technology required for building geostationary platforms for optical sensors is well-established thanks to the Meteosat and GOES (Geostationary Operational Environmental Satellite) series of meteorological sensors which have been operational since the 1970s. However, it is noted that the higher orbit required for geostationary platforms increases greatly the cost as compared to polar-orbiting platforms and gives a reduction in spatial resolution for the same optical system. Notwithstanding the cost issue, the potential for geostationary ocean colour is theoretically very high (Robinson *et al*., 2008) and plans for launching such sensors are at various stages of development within national and international space agencies (Kang *et al*., 2004; National Research Council, 2007). However, the concept has not yet been tested with real satellite data, which is the purpose of the present study.

Although dedicated geostationary ocean colour sensors do not yet exist in space, it is possible to make a feasibility study with the existing SEVIRI sensor on the METOSAT Second Generation platform (MSG). This sensor lacks sufficient bands for remote sensing of chlorophyll. However, it has been established previously for the Advanced Very High Resolution Radiometer (AVHRR) sensor (Stumpf and Pennock, 1989) that the use of a single broad red band, combined with a suitable near infrared band (for aerosol correction), is sufficient for quantification of TSM in turbid waters. In fact, TSM can be considered as quite an "easy" parameter to retrieve because of the strong signal: turbid regions can be identified in top of atmosphere radiance (Robinson, 1985) or even in photographs taken from space (Wolanski and Spagnol, 2003). Mapping of TSM is of interest in many turbid regions because of its link with sediment transport problems (dredging, dumping, geomorphology) (Fettweis *et al.*, 2006) and because of its impact on the availability of light for primary production (Ebenhoeh *et al.,* 1997). Remote sensing algorithms for TSM retrieval are now quite mature and satellite data is becoming more and more used in coastal monitoring and as support for modelling (Lacroix *et al.*, 2007). TSM has therefore been adopted for this feasibility study.

The specific objectives of this study are to test the feasibility of mapping TSM in the Southern North Sea using the SEVIRI sensor, to determine whether high frequency dynamics of TSM are detected and how/whether daily composites of TSM can be generated in partially cloudy weather. The SEVIRI sensor, test data set and processing algorithms, including atmospheric correction and one-band TSM retrieval are briefly described. Results are then presented for two cloud free days. Results show that (1) mapping of TSM in the Southern North Sea is feasible with SEVIRI and that TSM maps are well correlated with TSM maps obtained from MODIS (2) during cloud-free days, high frequency dynamics of TSM are detected. Finally, conclusions are drawn regarding the feasibility of geostationary ocean colour for mapping of TSM in coastal waters and recommendations are made for the design of future geostationary sensors for retrieval of both TSM and chlorophyll.

MATERIALS AND METHODS

SEVIRI instrument and test data sestet. The Spinning Enhanced Visible and InfraRed Imager (SEVIRI) radiometer (Muller, 2007), primarily designed to support operational meteorology applications like weather forecasting, has 11 spectral channels with a spatial resolution at nadir of 3km (5kmx6km at 52°N) and one visual broadband channel where the spatial resolution is 1km. The

nominal coverage includes the whole of Europe, all of Africa, a large part of the Atlantic Ocean and the Western Indian Ocean. Data is available in near real time every 15 minutes and operationally processed to level 1.5, *i.e.* corrected for radiometric and geometric non-linearity.

Two spectral bands were selected for TSM mapping: the red (0.560-0.710µm) and near-infrared (1.500-1.780µm) bands, at central wavelengths of 0.635 and 1.640µm, respectively. The 0.810µm band might be useful for TSM mapping, but the absorption by water vapour in this bands wavelength range (0.740-0.880µm) is very strong. An image test data set covering 15 consecutive days in September 2006 was obtained from the SEVIRI archive of the Royal Meteorological Institute of Belgium (RMIB).

Image processing steps. Sunlight reaching the SEVIRI sensor does not come entirely from the sea. Depending on turbidity, between 35% and 95% of the measured light flux can have an atmospheric origin. These atmospheric influences need to be eliminated from the total signal (ρ_{tot}^{TOA}) to obtain the water-leaving reflectance (ρ_w^{0+}). In this study, a simple atmospheric correction algorithm is used, based on the assumption that light reaching the sensor has undergone only one single scattering event. The main steps in this single scattering atmospheric correction are: (1) correction for absorption by atmospheric gasses, such as ozone, (2) correction for scattering by air molecules (Rayleigh scattering) and (3) correction for scattering by aerosols. The Rayleigh scattering is mainly dependent on wavelength and satellite geometry and can be calculated with precision, while the aerosol reflectance is highly variable in time and space. Aerosol correction is done by subtracting the Rayleigh corrected reflectance in the 1.6µm near infrared band, where the ocean is considered as perfectly black. TSM is then estimated from the water-leaving reflectance in the 0.6µm band. All image processing was performed in the MATLAB R2008a computing environment.

The water-leaving reflectance ρ_w^{0+} in the 0.6µm band, the signal to be retrieved, can be obtained from the total TOA reflectance ρ_{tot}^{TOA} as the sum of several contributions* (Viollier *et al.*, 1980; Gordon and Wang, 1994b):

$$\rho_{tot}^{TOA} = \rho_r^{TOA} + \rho_a^{TOA} + \rho_{ra}^{TOA} + \rho_{wc}^{TOA} + \rho_g^{TOA} + T_r T_a \rho_w^{0+}$$

where ρ_r^{TOA} is the contribution to the reflectance from scattering solely by air molecules, ρ_a^{TOA} is the reflectance resulting from scattering solely by aerosols, ρ_{ra}^{TOA} is the interaction term between molecular and aerosol scattering, ρ_{wc}^{TOA} is the reflectance from foam and white caps and ρ_g^{TOA} is the contribution from sun glint for which the only scattering event is specular reflection of direct sunlight. Sunglint reaches the sensor only for viewing zenith angles (θ_v) close to the sun zenith (θ_0) and for relative azimuth angles between sun (ϕ_0) and sensor (ϕ_v) close to 180°. The northern limit of our study area (see Figure 1) corresponds to a maximum SEVIRI satellite viewing angle of 64°. Rayleigh reflectances start to dominate the water-leaving signal (typically around 0.02 for moderately turbid waters) for larger viewing angles (see Figure 2), rendering data unusable for ocean applications. SEVIRI relative

* assuming ρ_w^{0+} to be relatively uniform over horizontal distances of at least several kilometres, this is not the case for areas very close to the coast (Viollier et al., 1980)

azimuth angle ($|\phi_0 - \phi_v|$) varies between 2 and 75° and θ_v ranges between 55° and 64° over the entire study area and in the timeframe 08:00-16:00 UTC. Measurements are clearly made outside the directions contaminated by sun glint and therefore ρ_g^{TOA} can be neglected. ρ_{wc}^{TOA} is also neglected in this approach, since this term is small for wind speeds lower than 10 m/s and largely corrected for in the aerosol correction for maritime aerosols (Gordon and Wang, 1994a). The ρ_{ra}^{TOA} is zero in the single scattering case and can be grouped with ρ_a^{TOA} over the wavelengths (0.635 to 1.640µm) considered in the multiple scattering case. T_r and T_a are the two-way diffuse atmospheric transmittances of air molecules and aerosol particles, respectively.

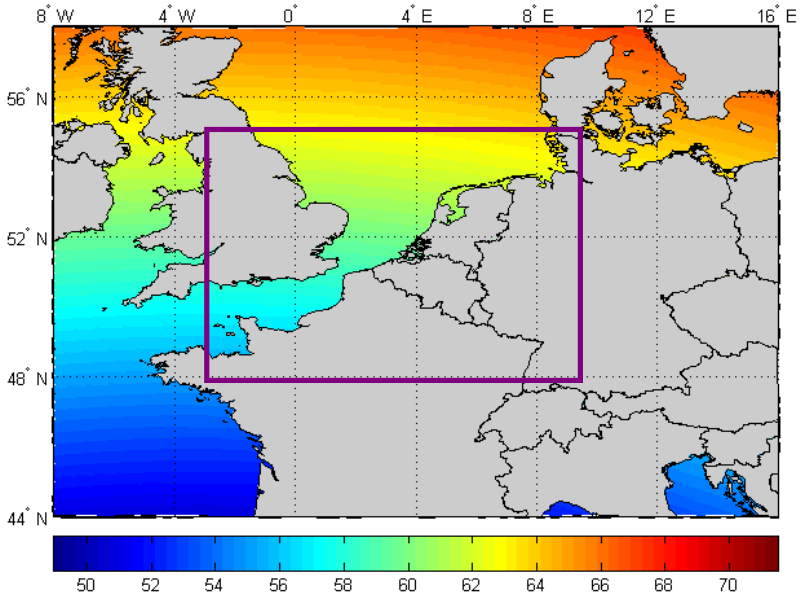

Figure 1. Viewing angle of SEVIRI (on MSG1 platform located at 3.5°W) over Western-Europe. The purple box delimits the study area, for which the northern limit corresponds to a 64° satellite viewing angle.

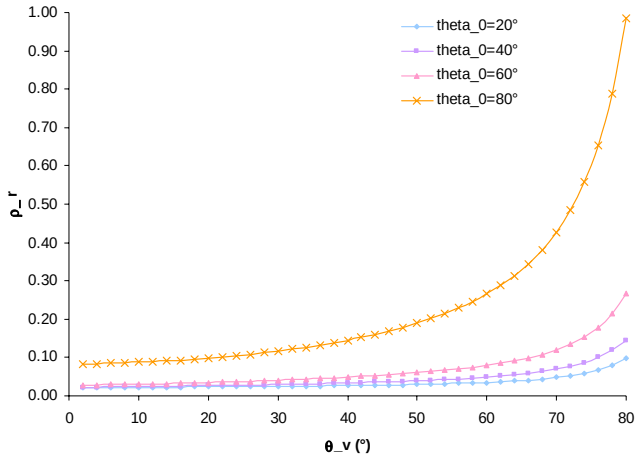

Figure 2. Rayleigh reflectance at 0.635µm for relative azimuth angles typical of SEVIRI ($\phi_0 - \phi_v = 30°$) and sun zenith angles of 20° (blue), 40° (purple), 60° (pink) and 80° (orange).

Calibration and ozone absorption correction. The SEVIRI level 1.5 count data (K) in the 0.6μm and 1.6μm bands were transformed into total radiance at the Top of Atmosphere (TOA) L_{tot}^{TOA} [in $Wm^{-2}sr^{-1}\mu m^{-1}$] by applying the calibration coefficients (c_f) and offset values (r_0), provided with the SEVIRI level 1.5 native format file headers, as follows:

$$L_{tot}^{TOA} = \frac{10(c_f K + r_0)}{\lambda_0^2} \qquad \text{(Govaerts and Clerici, 2004)}$$

where λ_0 is the band central wavelength.

Total radiance at TOA, L_{tot}^{TOA} was then converted to total reflectance at TOA:

$$\rho_{tot}^{TOA} = \frac{\pi d^2 L_{tot}^{TOA}}{E_0 \cos\theta_0} \qquad \text{(Govaerts and Clerici, 2004)}$$

where d is the Sun-Earth distance in astronomical units (AU), θ_0 is the sun zenith angle calculated from position, date and time (MATLAB algorithm by Reda and Andreas, 2003), E_0 is the extraterrestrial solar irradiance at TOA at 1AU (in $Wm^{-2}\mu m^{-1}$).

ρ_{tot}^{TOA} is corrected for ozone absorption by dividing it by the two-way ozone atmospheric transmittance $t_{oz}^{0,v}$:

$$t_{oz}^{0,v} = \mathrm{e}^{-k_\lambda U(\cos^{-1}\theta_0 + \cos^{-1}\theta_v)} \qquad \text{(Viollier } \textit{et al.}\text{, 1980)}$$

where k_λ is the ozone absorption coefficient ($k_{0.635\mu m} \approx k_{0.630\mu m}$=0.09 cm atm^{-1} and $k_{1.640\mu m}$=0 cm atm^{-1} from Neckel and Labs, 1981) and U is the ozone total column content (in cm atm). Daily ozone total column content was obtained from the SeaWiFS TOAST (Total Ozone Analysis using SBUV/2 and TOVS) data set and spatially averaged over the study area. Ozone concentrations of 0.292 cm atm and 0.295 cm atm were found on the 10th and the 21st of September 2006, respectively.

Rayleigh scattering correction. The single scattering Rayleigh reflectance, ρ_r^{TOA}, can be approximated as follows (Gordon *et al.*, 1988):

$$\rho_r^{TOA} = \frac{t_{oz}^{0,v} \tau_r p_r}{4\cos\theta_0 \cos\theta_v}$$

where τ_r is the Rayleigh scattering optical thickness and p_r is the Rayleigh scattering phase function. τ_r is computed as a function of wavelength λ (in μm), the actual atmospheric pressure P_{atm} at sea level and P_{atm0}=1013.25mbar, the standard atmospheric pressure:

$$\tau_r = \frac{P_{atm}}{P_{atm0}} 0.008569\lambda^{-4}(1+0.0113\lambda^{-2}+0.00013\lambda^{-4}) \qquad \text{(Hansen and Travis, 1974)}$$

The atmospheric pressure was obtained from 6-hourly data from the UK-METOffice atmospheric model nowcasts.

The Rayleigh scattering phase function, p_r is given by (Gordon and Wang, 1994b)

$$p_r = P_r(\theta_-) + \left[r_{sky}(\theta_0) + r_{sky}(\theta_v) \right] P_r(\theta_+)$$

where

$$P_r(\alpha) = \frac{3}{4}\left(1+\cos^2\alpha\right) \text{ and } \cos\theta_\pm = \pm\cos\theta_0\cos\theta_v - \sin\theta_0\sin\theta_v\cos(\phi_0-\phi_v)$$

The air/sea interface reflectance factor, $r_{sky}(\theta)$ is given by Fresnel's formula:

$$r_{sky}(\theta) = \frac{1}{2}\left[\left(\frac{\sin(\theta-\theta_t)}{\sin(\theta+\theta_t)} \right)^2 + \left(\frac{\tan(\theta-\theta_t)}{\tan(\theta+\theta_t)} \right)^2 \right]$$

with $\theta_t = \sin^{-1}\left(\frac{1}{n_w}\sin\theta \right)$ and n_w, the refraction index approximated by 1.34.

Aerosol scattering correction and diffuse atmospheric transmittance. The aerosol reflectance at TOA, ρ_a^{TOA} in the 0.6μm band can be obtained from the Rayleigh corrected reflectance in the 1.6μm band, where the ocean is considered as perfectly black (*i.e.* the water-leaving reflectance is zero). Doing so, we should take into account the wavelength dependence of ρ_a^{TOA} and the spatial and temporal variability of the spectral behaviour and size distribution of the aerosol particles, described by the Angstrom coefficient (α). Based on experience, it is reasonable to assume a fixed value of α over the entire scene and over an entire day. Furthermore, it is expected that ρ_a^{TOA} can be expressed as follows:

$$\rho_a^{TOA}(\lambda) = \rho_a^{TOA}(\lambda_0)\left(\frac{\lambda}{\lambda_0} \right)^{-\alpha}$$

Then, α can be obtained from the epsilon value for aerosol correction from the 765 and 865 nm MODIS bands. In the present study we will assume "white" aerosols, with α=0.

T_a is approximated by 1 and

$$T_r = \frac{(1+e^{-\tau_r \cos^{-1}\theta_v})(1+e^{-\tau_r \cos^{-1}\theta_0})}{4} \qquad \text{(Viollier et al., 1980)}$$

Single band TSM algorithm. The single band TSM retrieval algorithm of (Nechad *et al.*, 2003) has been recalibrated here for the broad SEVIRI 0.635µm band from an archive of 67 seaborne reflectance and TSM measurements to give:

$$TSM = \frac{A\rho_w^{0+}(0.6\mu m)}{C - \rho_w^{0+}(0.6\mu m)}$$

giving the coefficients A=38.92 mg/l and C=0.16. While this algorithm is defined for band-integrated reflectance, which can easily be related to band-integrated radiance for a narrow band sensor the relation between band-integrated reflectance and band-integrated radiance is less trivial for a broadband sensor. To show the applicability of the TSM algorithm to the broad red band, a correlation analysis between the upwelling radiance at the central wavelength of the 0.6µm band and the spectral integral of the upwelling radiance over the wavelength range of the 0.6µm band, convoluted with the SEVIRI spectral response curve, was performed. All available sea-borne data since 2004 (440 observations) were used in the regression analysis. The correlation coefficient was found to be 0.99987.

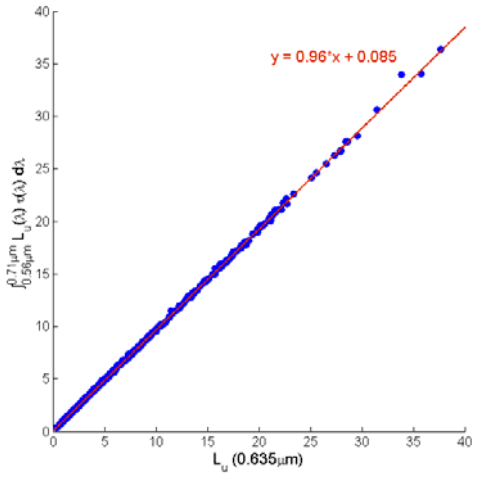

Figure 3. Linear regression between the upwelling radiance at the central wavelength of the red band ($L_u(0.635\mu m)$) and the spectral integral of the upwelling radiance over the wavelength range of the red band, convoluted with the SEVIRI spectral response curve $\tau(\lambda)$.

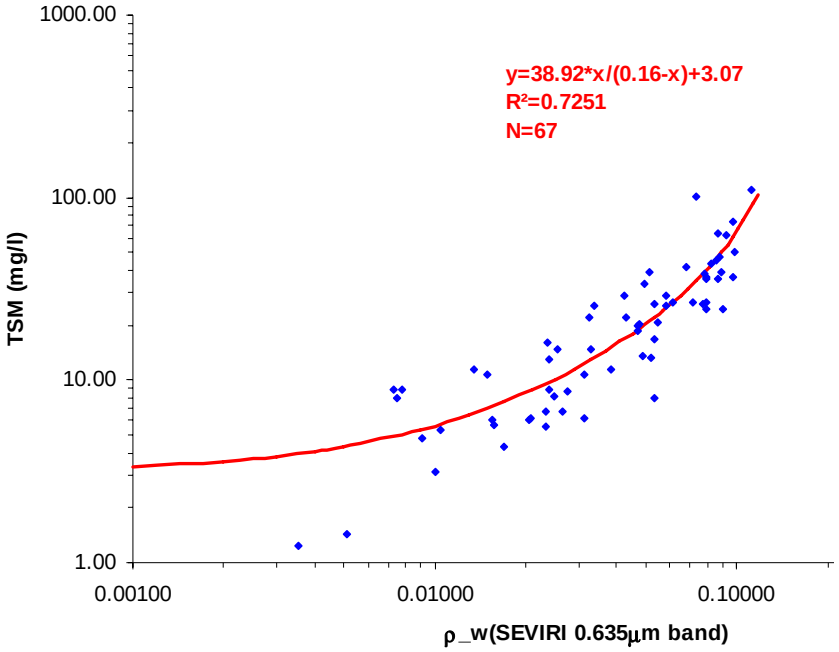

Figure 4. Regression between 67 seaborne reflectance measurements of ρ_w^{0+} in the SEVIRI 0.635µm band and TSM concentration.

Cross-validation. SEVIRI TSM products were cross-validated with MODIS TSM products on September 10th and 21st at 10:45 UTC and 12:30 UTC, respectively. MODIS TSM images were resampled to the larger SEVIRI grid computing the average TSM value of the centre MODIS pixel and its 8 neighbouring pixels. Post-processing of the resampled MODIS TSM image and the SEVIRI TSM image included removing isolated TSM pixels (*e.g.* isolated TSM values in a cloud) and applying a one pixel wide buffer to clouds and land. A log-log regression analysis of MODIS TSM values against SEVIRI TSM values was made, discarding TSM values smaller than 3 mg/l, which are considered close to the detection limit of in-situ measurements used for algorithm calibration.

RESULTS AND DISCUSSION

TSM concentration mapping. Figure 5 shows TSM concentrations in the Southern North Sea obtained from SEVIRI on September 10th at 10:00 UTC. These distributions are similar to those found in many previous studies based on *in situ* measurements, e.g. (Eisma, 1981), or satellite measurements from CZCS (Holligan *et al.*, 1989), AVHRR (Van Raaphorst *et al.*, 1998), SeaWiFS (Eleveld *et al.*, 2004), MODIS or MERIS (Ruddick *et al.*, 2008). TSM concentrations are lower (<20mg/l) offshore in the Central North Sea and the English Channel.

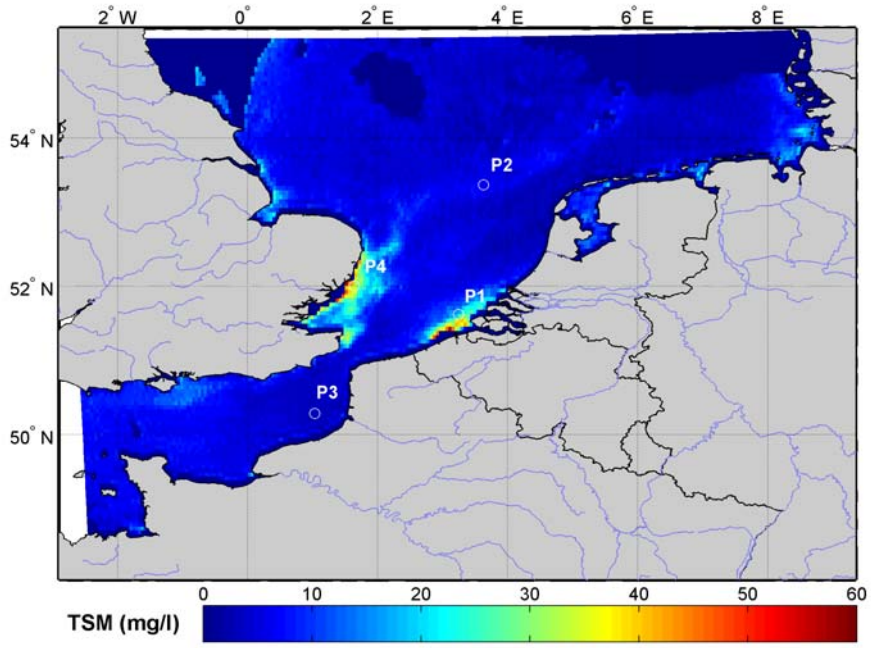

Figure 5. TSM concentration in the Southern North Sea on September 10th 2006 at 10:00 UTC. Four pixels P1-P4 were selected in clear and turbid waters for which high frequency TSM dynamics are presented later.

Cross-validation of TSM maps. Figure 6 and Figure 8 show a spatial comparison between SEVIRI TSM and MODIS TSM maps, captured almost simultaneously on September 10th and 21st 2006, respectively. These products show comparable spatial patterns and comparable TSM ranges. A cross-validation analysis was performed between corresponding TSM products and the resulting log-log regressions are shown in Figure 7 (for September 10th 2006) and Figure 9 (for September 21st 2006). A good correlation was found in both cases with correlation coefficients of 0.8294 and 0.7721, respectively. It is noted that the slope of the regression line is not equal to one. This could be caused by a non-zero offset in the MODIS TSM algorithm, the rather crude cloud mask applied, masking high reflectances in the 0.6µm band or by differences in atmospheric correction.

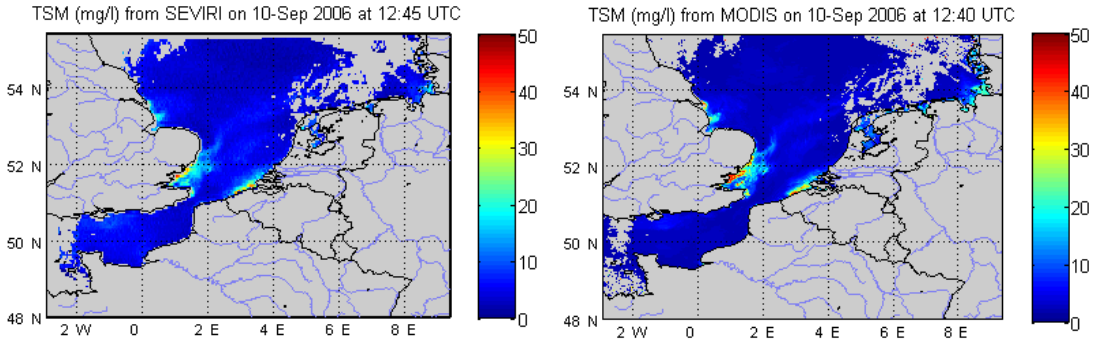

Figure 6. TSM maps obtained from SEVIRI (left) and MODIS (right) on September 10th at 12:45 UTC and 12:40 UTC, respectively.

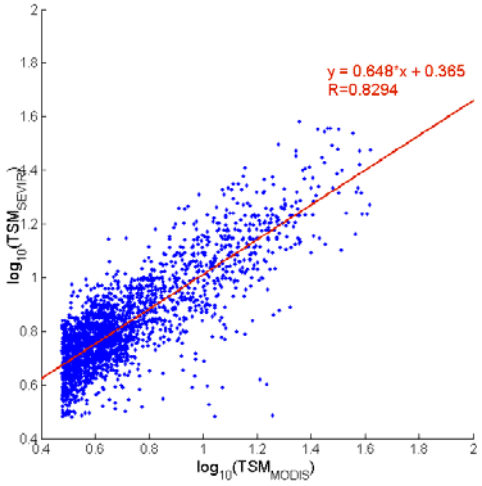

Figure 7. Log-log regression of TSM obtained from MODIS and TSM obtained from SEVIRI on September 10th 2006 at 12:45 UTC and 12:40 UTC, respectively. Values below 3 mg/l were discarded.

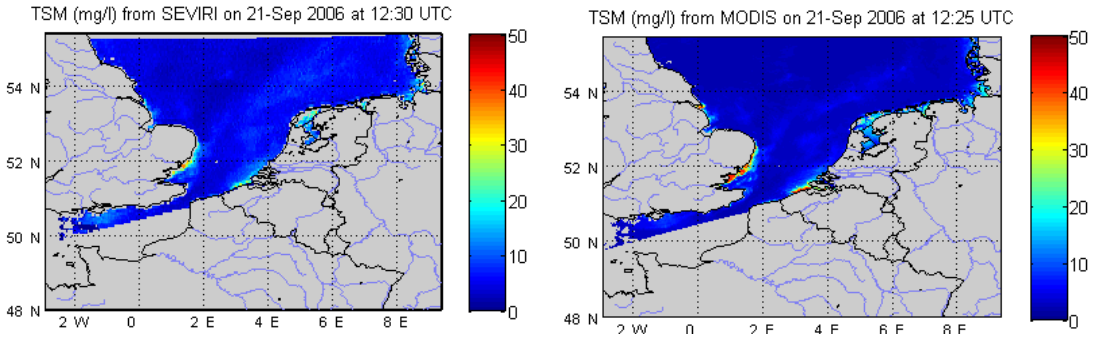

Figure 8. TSM maps obtained from SEVIRI (left) and MODIS (right) on September 21st at 12:30 UTC and 12:25 UTC, respectively.

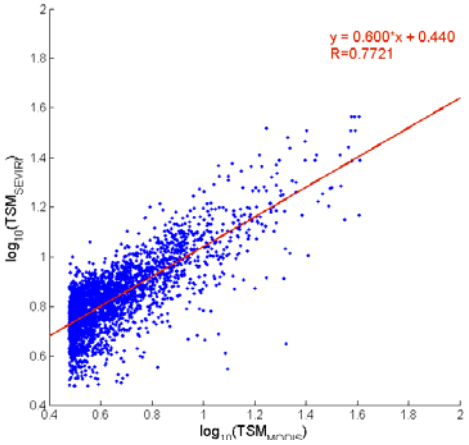

Figure 9. Log-log regression of TSM obtained from MODIS and TSM obtained from SEVIRI on September 21st 2006 at 12:30 UTC and 12:25 UTC, respectively. Values below 3 mg/l were discarded.

High frequency TSM dynamics. The high frequency variability of TSM concentration is studied on a cloudfree day on September 10th 2006 at four different pixels/stations (stations shown on Figure 5) in clear and turbid waters of the Southern North Sea: P1 close to the mouth of river Scheldt (turbid water), P2 in the Middle of the North Sea (moderately turbid water), P3 offshore of Calais in clear waters and P4, offshore of Lowestoft, again in more turbid waters. TSM time series were extracted at these four pixels between 8:00 and 16:00 UTC and are shown in Figure 10. Outside this timeframe, low sun angles cause the Rayleigh reflectance to obscure the water leaving signal. A time series was also extracted for the eastern neighbour pixel of each selected pixel (denoted Pi_nb) to allow to check for spatial consistency of TSM dynamics.

The variability of TSM concentration in the coastal pixels P1 and P4 suggests a periodicity possibly related to the tidal cycle. This periodicity is not observed for pixels further offshore (P2 and P3), which suggests that it is not an artifact introduced by image processing. Comparison of the TSM dynamics between neighbouring pixels shows its spatial consistency. The noise in the time series can possibly be reduced if the atmospheric correction algorithm is improved. For example, the 1.6µm band used for aerosol correction is quite noisy. This improved correction algorithm should take into account:

1. the spatial and temporal variability of the spectral behaviour and size distribution of aerosol particles
2. the impact of aerosol and Rayleigh scattering on atmospheric transmittance
3. the absorption of light by atmospheric gasses, other than ozone, like water vapour, methane and carbon dioxide.
4. Multiple scattering events

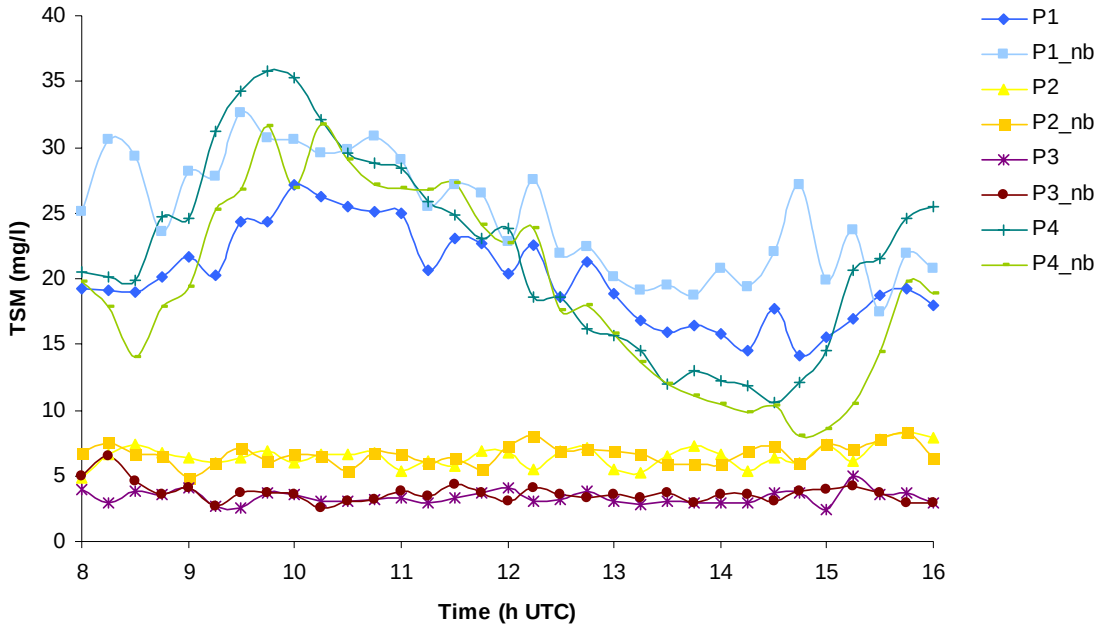

Figure 10. High frequency variability of TSM concentration at four selected pixels and their Eastern neighbour pixel (Pi_nb).

CONCLUSION AND FUTURE PROSPECTS

This study demonstrates the feasibility of the SEVIRI radiometer for TSM mapping and provides the basis for future mapping of TSM from geostationary sensors at very high temporal resolution. Important applications of the availability of very high temporal resolution TSM maps include:

1. Mitigating the problems of cloudiness encountered with the current generation of polar-orbiters (MODIS, MERIS, SeaWiFS), through daily averaging of the SEVIRI images.
2. Studying high frequency dynamics of the coastal ecosystem: resuspension of bottom sediments.
3. Studying the relationship between TSM, the amount of light available for photosynthesis by phytoplankton and the timing of the spring phytoplankton bloom. High concentrations of TSM and high water turbidity reduce the sunlight available to phytoplankton for photosynthesis, and thus plays an important role in the timing of the algal spring bloom.
4. Identifying areas of high frequency variability of TSM, indicating where the SeaWiFS/MODIS/MERIS daily products are less reliable.

The present paper describes a preliminary processing algorithm which is sufficient to establish feasibility of the technique but should be improved in many respects to obtain higher quality products. In particular, improvements to the atmosphere correction should include:

- consideration of absorption by gases other than ozone (especially water vapour in the 0.8µm band) as well as the effect of scattering on atmospheric transmittances,
- a more precise calculation of Rayleigh reflectance based on radiative transfer simulation and,
- consideration of non-white aerosols, possibly using the 0.8µm and taking information on daily aerosol reflectance spectral variation from external information (e.g. MODIS imagery, an aerosol climatology, sunphotometer data and/or a combination of the 0.8µm and 1.6µm bands).

In addition the SEVIRI processing could be extended to a higher spatial resolution by use of the panchromatic visual band. This would require further refinement of both the atmospheric correction and the TSM retrieval algorithms.

More generally, this feasibility study for SEVIRI can serve as a basis for design of future geostationary ocean colour missions for quantification of chlorophyll *a*. This would require additional spectral bands for chlorophyll *a* retrieval, better radiometric sensitivity and more accurate atmospheric correction. However, there should be no significant algorithmic difficulties since the methodology for polar-orbiting sensors is easily transported to geostationary sensors – the stable geostationary viewing geometry even simplifies some aspects of atmospheric correction. The potential for geostationary ocean colour is both enormous (Robinson et al., 2008) and is now clearly feasible.

ACKNOWLEDGEMENTS

This research was supported by the BELCOLOUR-2 project, funded by the STEREO programme of the Belgian Science Policy Office under contract SR/00/104. We thank Pierre-Yves Deschamps for the idea of using SEVIRI, Nicolas Clerbaux (Royal Meteorologic Institute of Belgium) for providing SEVIRI data and Didier Ramon and Emilien Bernard for the scientific discussions concerning the SEVIRI atmospheric correction.

REFERENCES

Ebenhoeh, W., J. G. Baretta Bekker, and J. W. Baretta. 1997. The primary production module in the marine ecosystem model ERSEM II, with emphasis on the light forcing. J. Sea Res. **38:** 173-193.

Eisma, D. 1981. Supply and deposition of suspended matter in the North Sea. Spec. Publs int. Ass. Sediment **5:** 415-428.

Eleveld, M. A., R. Pasterkamp, and H. J. Van Der Woerd. 2004. A survey of total suspended matter in the Southern North Sea based on 2001 SeaWiFS data. EARSeL eProceedings **3:** 166-178.

Fettweis, M., F. Francken, V. Pison, and D. Van Den Eynde. 2006. Suspended particulate matter dynamics and aggregate sizes in a high turbidity area. Marine Geology **235:** 63-74.

Gordon, H.R. J.W., Brown, and R.H. Evans. 1988. Exact Rayleigh scattering calculations for use with the Nimbus-7 Coastal Zone Color Scanner. Applied Optics **27**: 862-871

Gordon, H. R., and M. Wang. 1994a. Influence of oceanic whitecaps on atmospheric correction of ocean-color sensors. Applied Optics **33:** 7754-7763.

Gordon, H. R., and M. Wang. 1994b. Retrieval of water-leaving radiance and aerosol optical thickness over the oceans with SeaWiFS: a preliminary algorithm. Applied Optics **33:** 443-452.

Govaerts Y., and M. Clerici, 2004. MSG-1/SEVIRI Solar Channels Calibration Commissioning Activity Report. EUMETSAT document number EUM/MSG/TEN/04/0024.

Hansen, J.E., and L.D. TRavis. 1974. Light scattering in planetary atmospheres. Space Science Reviews **16:** 527-610.

Holligan, P. M., T. Aarup, and S. B. Groom. 1989. The North Sea satellite colour atlas. Continental Shelf Research **9:** 665-765.

International Ocean Colour Coordinating Group (Ioccg). 2000. Remote sensing of ocean colour in coastal, and other optically-complex waters, p. 140. IOCCG.

Kang, G., S. Kang, S. Yong, J. Kim, Y. Chang, and H. Youn. 2004. Korea Geostationary Ocean Color Imager, p. 3261-3263. IGARSS. IEEE.

Lacroix, G., K. Ruddick, Y. Park, N. Gypens, and C. Lancelot. 2007. Validation of the 3D biogeochemical model MIRO&CO with field nutrient and phytoplankton data and MERIS-derived surface chlorophyll *a* images. Journal of Marine Systems **64(1-4):** 66-88.

Muller, J., 2007. MSG Level 1.5 Image Data Format Description. EUMETSAT technical document number EUM/MSG/ICD/105 (available on: http://www.eumetsat.int/Home/Main/Publications/Technical_and_Scientific_Documentation/Technical_Notes/SP_1124282611560)

National Research Council. 2007. Earth science and applications from space: national imperatives for the next decade and beyond. National Academy of Sciences.

Nechad, B., V. De Cauwer, Y. Park, and K. Ruddick. 2003. Suspended Particulate Matter (SPM) mapping from MERIS imagery. Calibration of a regional algorithm for the Belgian coastal waters. MERIS user workshop, 10-13th November 2003. European Space Agency.

Neckel, H. and D. Labs.1981. Improved Data for Solar Spectral Irradiance from 0.33 to 1.25 micrometers. Solar Physics 74:231-249. (available on: http://rredc.nrel.gov/solar/pubs/spectral/model/t2-1.html)

Reda, I. and A. Andreas. 2003. Solar position algorithm for solar radiation application. National Renewable Energy Laboratory (NREL). Technical report NREL/TP-560-34302.

Robinson, I. S. 1985. Satellite Oceanography. Ellis Horwood.

Robinson, I. S., D. Antoine, M. Darecki, P. Gorringe, L. Pettersson, K. Ruddick, R. Santoleri, H. Siegel, P. Vincent, M. R. Wernand, G. Westbrook, and G. Zibordi. 2008. Remote sensing of shelf sea ecosystems: state of the art and perspectives, p. 60. European Science Foundation Marine Board.

Ruddick, K., G. Lacroix, C. Lancelot, B. Nechad, Y. Park, S. Peters, and B. Van Mol. 2008. Optical remote sensing of the North Sea, p. 79-90. *In* V. Barale and M. Gade [eds.], Remote sensing of the European Seas. Springer-Verlag.

Stumpf, R. P. 2001. Applications of satellite ocean color sensors for monitoring and predicting harmful algal blooms. Human and Ecological Risk Assessment **7:** 1363-1368.

Stumpf, R. P., and J. R. Pennock. 1989. Calibration of a general optical equation for remote sensing of suspended sediments in a moderately turbid estuary. Journal of Geophysical Research **94:** 14363-14371.

Viollier, M., D. Tanré, and P.Y. Deschamps, 1980. An algorithm for remote sensing of water color from space. Boundary Layer Meteorology **18:** 247-267.

Van Raaphorst, W., C. J. M. Philippart, J. P. C. Smit, F. J. Dijkstra, and J. F. P. Malschaert. 1998. Distribution of suspended particulate matter in the North Sea as inferred from NOAA/AVHRR reflectance images and in situ observations. Journal of Sea Research **39:** 197-215.

Wolanski, E., and Spagnol. 2003. Dynamics of the turbidity maximum in King Sound, tropical Western Australia. Estuar Coast Mar Sci **56:** 877-890.